Multiple electromechanically-induced-transparency windows and Fano resonances in hybrid nano-electro-optomechanics

Kamran Ullah*
Department of Physics, Quaid-i-Azam University, 45320 Islamabad, Pakistan

Hui Jing†
Department of Physics, Hunan Normal University, Changsha 410007, People's Republic of China

Farhan Saif‡
Department of Electronics, Quaid-i-Azam University, 45320 Islamabad, Pakistan

(Received 18 July 2017; published 12 March 2018)

We show multiple electromechanically-induced transparency (EMIT) windows in a hybrid nano-electro-optomechanical system in the presence of two-level atoms coupled to a single-mode cavity field. The multiple EMIT-window profile can be observed by controlling the atom field coupling as well as Coulomb coupling between the two charged mechanical resonators. We derive the analytical expression of the multiple-EMIT-windows profile and describe the splitting of multiple EMIT windows as a function of optomechanical coupling, atom-field coupling, and Coulomb coupling. In particular, we discuss the robustness of the system against the cavity decay rate. We compare the results of identical mechanical resonators to different mechanical resonators. We further show how the hybrid nano-electro-optomechanics coupled system can lead to the splitting of the multiple Fano resonances (MFR). The Fano resonances are very sensitive to decay terms in such systems, i.e., atoms, cavities, and the mechanical resonators.

DOI: 10.1103/PhysRevA.97.033812

I. INTRODUCTION

Mechanically induced transparency (MIT) arises in an optomechanical system due to the mechanically moving end mirror. It is a quantum interference phenomenon by which a narrow absorption and transmission window is created [1]. Electromagnetically induced transparency (EIT) was first reported theoretically [2] and experimentally studied in strontium vapor by Boller *et al.* [3], in lead vapor by Field *et al.* [4], and in optical cavity by Weis [5]. In many schemes EIT has been studied such as Bose Einstein condensate (BEC) [6], in solid state demonstrated in quantum wells [7], quantum dots [8], metamaterial [9], and nitrogen vacancy centers [10]. Recently, EIT is observed experimentally in a classical system via coupled RLC circuits [11,12].

Moreover, EIT is also observed in atomic gas Sr having Λ-type three-level atomic structure [3] as the destructive interferences of two dressed states in Sr atom exhibits an EIT phenomenon. Like the optomechanical system, in the Sr atom a photon energy level and the first-order sideband energy level behave like a Λ-type three-level structure [5]. In addition, the transition of a two-mode polariton coupled system also behaves like a Λ-type three-level structure and is related to the MIT effect [13]. Recently, in an optomechanics setup assisted with a Γ-type atomic system coherent quantum-noise cancellation and optomechanical cooling [14] have been reported. More recently, Huang and Tsang [15] have also shown multiple MIT windows with N number of membranes in optomechanics.

In the optomechanical system the mechanical resonators (MR_s) are treated in different ways such as the demonstration with other quantum objects [16], electron spin [17], phonon blockade [18], and high harmonic generation [19]. The combination of mechanical resonators with the optical cavity is called the optomechanical system [20–22], in which the MR_s are coupled to the cavity field causing radiation pressure and hence the out field exhibits the mechanically induced transparency (MIT). The slow and fast light [23], normal mode splitting [24–30], quantum information transfer [31], entanglement [32,33], realization of classical chaos [34], and quantum chaos in nanocavities [35,36] are other applications of the radiation pressure in an optomechanical system. Recently, inverse electromagnetic-induced transparency is also observed in a single-mode cavity field in the optomechanical system [37]. Hence, the combination of an optomechanical system with quantum electrodynamics leads to a hybrid optomechanical system [38] influencing the electrical-induced transparency due to the additional medium of atoms, which has been studied in detail [39].

The quantum nature of the electronic circuit together with the macroscopic degree of freedom of the mechanical oscillator of the optomechanical system is a fascinating research domain. Therefore, the mechanical resonator MR_1 of an optomechanical system is coupled to another external mechanical resonator MR_2 connected to the bias voltages V_1 and V_2 called the electro-optomechanical system. Due to electrostatic Coulomb

*kamran@phys.qau.edu.pk
†jinghui73@foxmail.com
‡farhan.saif@fulbrightmail.org

interaction the EMIT window splits from single to double windows [40,41]. The significance of the bias voltage is to control the Coulomb interaction between the mechanical resonators [41,42]. It leads one to explore the optomechanical system in multiple-channel electrical-induced transparency with electrostatic Coulomb interaction. Whenever, a coherent weak probe field is applied to the cavity of an optomechanical system, the mechanical resonator behaves like a switch that controls the probe photon transmission such that photons can pass through the cavity one by one [43–45] or two by two [46] in the limit of the strong single-photon optomechanical interaction [47–49].

Among these applications, Fano line shapes are the most prominent phenomenon occurring in the optomechanical system. The Fano line profile has an asymmetry shape produced by the scattering of light amplitude. Scattering interferences were first theoretically studied by Fano and he wrote a series of papers by assuming a grating consisting of lossy dielectric material, and suggesting that anomalies could be associated with the excitation of a surface wave along the grating [50]. But the most fascinating thing is that the theoretical formula was fit in inelastic scattering of electron from noble gas (helium atom) [51]. In the optomechanical system the Fano line shape was recently studied by Qu and Agarwal [52]. Fano resonances played an important role in the fields of plasmonics [53,54], photonics crystal [55–57], nanoparticles [58], in graphene [59,60], and improvement of the efficiency of heat engines [61]. Moreover, the asymmetry of the Fano line shapes can be controlled by the saturation rate of two interference paths [62]. Since the results of multiple electromagnetically induced transparency is the manifestation of Fano resonances and can be described from the output field of the system by using the multiple electrically-induced-transparency approach. Recently, the EMIT in a nano-electromechanical system with the resonator of Nb/Si_3N_4 clamped at both end bilayers to increase the resonant frequency and the quality factor of the mechanical oscillator is discussed by Fredrik Hocke *et al.* [63]. In this paper, we consider a nano-electro-optomechanical system (NEOMS) for multiple electromechanical-induced transparency (EMIT), in which the two mechanical resonators MR_1 and MR_2 are connected to external bias voltages V_1 and V_2. Both mechanical resonators are charged due to V_1 and V_2 and generate the Coulomb coupling between MR_1 and MR_2. There are N numbers of two-level ultracold atoms loaded between MR_1 and the cavity field. Due to the atom field interaction the electrical-induced transparency of the two-window profile split into the three-window profile. Our proposed hybrid electro-optomechanical system is sketched in Fig. 1 in which the first resonator MR_1 is coupled to the cavity field as well as to the second resonator MR_2. The importance of the bias voltages is to control the Coulomb interaction between the resonators. Hybridized systems, albeit having more elements, have the new advantage of combing different physical systems to achieve novel features which are hard or even impossible by steering any single element [16,64]. For this reason a comparison between our hybrid nano-electo-optomechanical system (NEOMS) with the previous simple optomechanical system of the single EMIT window [65–67] and double EMIT windows [68–71] shows some advantages: (i) Two output lights with different frequencies are controlled by a single driving light frequency. (ii) Our system is robust against the cavity decay rate, as a result narrow EMIT windows profile is observed. (iii) The EMIT windows profile of the system directly depends on the Coulomb coupling. (iv) The atom field coupling plays a vital role in triple EMIT windows splitting, however, both couplings directly influence the multiple-EMIT-windows profile and break the symmetry of the system for very large values. This paper comprises the following sections: In Sec. II, we introduce the theoretical model. In Sec. III, we discuss the dynamics of the system and solve the system using quantum Heisenberg-Langevin's picture. In Sec. IV, we discuss the multiple EIT windows profile of the absorption and dispersion spectra of the system. In addition, we explain the robustness of the system against the cavity decay rate corresponding to identical mechanical resonators (MR_s). In Sec. V, we treat the mechanical resonators (MR_s) differently and compare the results to the former results. In Sec. VI, we discuss the multiple Fano resonances (MFR). Finally, in Sec. VII, we conclude our results.

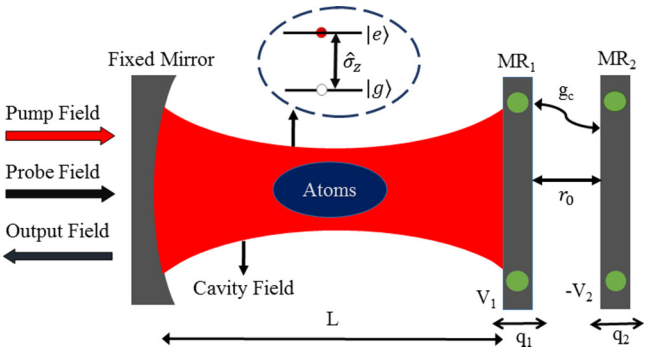

FIG. 1. Schematic demonstration of the nano-electro-optomechanical system contains N_a identical trapped two-level atoms. The MR_1 is coupled to the cavity field and external mechanical resonator MR_2 as well. The MR_1 is charged by bias voltage V_1 and MR_2 is charged by bias voltage $-V_2$, where g_c is the Coulomb coupling between the two resonators. The cavity mode is driven by a strong input laser field and weak probe field through the fixed mirror, where L is the cavity length, σ_z is the transition operator between the two levels, and r_0 is the equilibrium distance between MR_1 and MR_2.

II. EXPERIMENTAL SETUP

The model consists of an ensemble of N_a number of two-level ultracold atoms inside a Fabery Pérot cavity of length L, a fixed mirror and mechanical resonators (MR_s) as shown in Fig. 1. The mechanical resonators consist of two charged mirrors. The first mechanical resonator (MR_1) is coupled to the cavity field via optomechanical coupling g_0, and also coupled with another mechanical resonator (MR_2) electrostatically by a Coulomb interaction g_c. A high intense laser field of amplitude E_l and a weak probe field of amplitude ϵ_p are sent inside the cavity. The external bias voltages V_1 and V_2 are provided to the mechanical resonators by which we control the Coulomb coupling. The first mechanical resonator is charged by bias voltage V_1 while the second mechanical resonator is charged by a bias voltage V_2. In addition, the two-level atoms are off-resonantly coupled by a Tavis-Cummings-type interaction to the optical

field [72]. The Hamiltonian of the whole system reads as

$$H = \hbar\omega_c c^\dagger c + \frac{1}{2}\sum_{i=1}^{N}\hbar\omega_a\sigma_z^{(i)} + \left(\frac{p_1^2}{2m_1} + \frac{1}{2}m_1\omega_1^2 q_1^2\right) + \left(\frac{p_2^2}{2m_2} + \frac{1}{2}m_2\omega_2^2 q_2^2\right) - \hbar g_0 c^\dagger c q_1 + \hbar g_{ac}\sum_{i=1}^{N}(\sigma_+^{(i)}c + \sigma_-^{(i)}c^\dagger) + \hbar g_c q_1 q_2 + i\hbar E_l(c^\dagger e^{-i\omega_l t} - \text{H.c.}) + i\hbar(c^\dagger\epsilon_p e^{-i\omega_p t} - \text{H.c.}), \quad (1)$$

where the first term is for the single-mode cavity field, and the second term is for the atomic transition with atomic frequency ω_a. The third and fourth terms represent the oscillations of MR_1 and MR_2 with effective masses m_1 and m_2. The fifth term represents the optomechanical coupling between the cavity field and charged MR_1 given by $g_0 = \frac{\omega_c}{L}\sqrt{\frac{\hbar}{m_1\omega_1}}$. The sixth term comes due to interaction between field and atoms and it is related to the cavity mode volume and the dipole moment of the atomic transition. i.e., $g_{ac} = \mu\sqrt{\frac{\omega_a}{2\hbar\epsilon_0 V}}$. The seventh term represents the Coulomb coupling between the charged resonators MR_1 and MR_2. The charge on MR_1 is C_1V_1 while on MR_2 it is $-C_2V_2$ with capacitors C_1 and C_2 corresponding to bias voltages V_1 and $-V_2$. The Coulomb coupling between MR_1 and MR_2 is defined as $g_c = \frac{C_1V_1C_2V_2}{2\pi\hbar\epsilon_0 r_0^3}$ [41,74–76], where, r_0 is the equilibrium distance between MR_1 and MR_2. The last two terms represent the input laser field and the probe field with amplitudes E_L and ϵ_p. Here, $E_l = \sqrt{\frac{2\wp_l\kappa}{\hbar\omega_l}}$ and $\epsilon_p = \sqrt{\frac{2\wp_p\kappa}{\hbar\omega_p}}$, and $\wp_l$ and $\wp_p$ are the laser and probe field powers. Moreover, c and $c^\dagger$ are the annihilation and creation operators of the cavity field, p_1 and p_2 are the momentum operators of MR_1 and MR_2 while q_1 and q_2 are the position operators of MR_1 and MR_2. The symbols σ_z^i, σ_+^i, and σ_-^i are the Pauli-spin matrices that satisfy the spin matrix algebra i.e., $[\sigma_\pm^i,\sigma_\mp^i = \pm\sigma_z^i]$ and $[\sigma_z^i,\sigma_\pm^i = \pm 2\sigma_\pm^i]$. We introduce new bosonic operators for the atom in terms of annihilation and creation, i.e., $a = \frac{\sigma_-}{\sqrt{|\langle\sigma_z\rangle|}}$, $a^\dagger = \frac{\sigma_+}{\sqrt{|\langle\sigma_z\rangle|}}$, with the bosonic commutation relation $[a,a^\dagger] = 1$ [73]. At ground state atoms satisfy the relation $\langle\sigma_z^i\rangle = -N_a$ and cannot change by the interaction with the cavity. Rotating the frame with the laser frequency ω_l the Hamiltonian of the whole system becomes

$$H = \hbar\Delta_c c^\dagger c + \hbar\Delta_a a^\dagger a + \left(\frac{p_1^2}{2m_1} + \frac{1}{2}m_1\omega_1^2 q_1^2\right) + \left(\frac{p_2^2}{2m_2} + \frac{1}{2}m_2\omega_2^2 q_2^2\right) - \hbar g_0 c^\dagger c q_1 + \hbar g_{ac}\sqrt{N_a}(a^\dagger c + a c^\dagger) + \hbar g_c q_1 q_2 + i\hbar E_l(c^\dagger - c) + i\hbar(c^\dagger\epsilon_p e^{-i\delta t} - c\epsilon_p^\star e^{i\delta t}), \quad (2)$$

where $\Delta_c = \omega_c - \omega_l$ and $\Delta_a = \omega_a - \omega_l$ are the detuning between the field frequency and atomic frequency with respect to laser frequency, and δ is the detuning between the probe field with frequency ω_p and the strong driving field with frequency ω_l.

III. THEORETICAL MODEL AND SOLUTIONS OF NEOMS

In order to study the complete dynamics of the system, we introduce new terms, which are associated with the dissipation of the system. Let γ_1 and γ_2 be the decay terms corresponding to MR_1 and MR_2; γ_a is the decay term due to the atomic oscillation between the two levels. The Heisenberg-Langevin equations for the system described as

$$\begin{aligned}
\dot{q_1} &= \frac{p_1}{m_1},\\
\dot{q_2} &= \frac{p_2}{m_2},\\
\dot{p_1} &= -m_1\omega_1^2 q_1 + g_0 c^\dagger c - g_c q_2 - \gamma_1 p_1 + \zeta_1(t),\\
\dot{p_2} &= -m_2\omega_2^2 q_2 - g_c q_1 - \gamma_2 p_2 + \zeta_2(t),\\
\dot{c} &= -(\kappa + i\Delta_c)c + i g_0 c q_1 - i g a + E_l + \epsilon_p e^{-i\delta t} + \sqrt{2\kappa}c_{\text{in}}(t),\\
\dot{a} &= -(\gamma_a + i\Delta_a)a - i g c + \sqrt{2\gamma_a}a_{\text{in}}(t),
\end{aligned} \quad (3)$$

where $\hbar = 1$ and $g = g_{ac}\sqrt{N_a}$. Moreover, $\zeta_1(t)$ is the quantum Brownian thermal noise term that comes from the coupling between the cavity field and MR_1, while $\zeta_2(t)$ is the quantum Brownian noise term that comes from the Coulomb coupling between MR_1 and MR_2, κ is the decay of the cavity field, and c_{in} is the input vacuum noise operator with zero mean values, i.e., $\langle c_{in}\rangle = \langle\zeta(t)\rangle = 0$ [77]. They follow the nonvanishing commutation relations $\langle\delta\hat{c}_{\text{in}}(t)\delta c_{\text{in}}(t')\rangle = 0$, $\langle\delta c_{\text{in}}(t)\delta c_{\text{in}}^\dagger(t')\rangle = \delta(t-t')$ and $\langle\zeta(t)\zeta(t')\rangle = (n+1)\delta(t-t')$ [78]. Here, $n = (e^{\frac{\hbar\omega_{1,2}}{2K_BT}} - 1)^{-1}$ is the equilibrium occupation number of the resonators having frequency $\omega_{1,2}$, k_B is the Boltzmann constant, and T is the thermal bath temperature. Under the mean field approximation $\langle c^\dagger c\rangle = \langle c^\dagger\rangle\langle c\rangle$ [1], the mean value equations of the system become

$$\begin{aligned}
\langle\dot{q_1}\rangle &= \frac{\langle p_1\rangle}{m_1},\\
\langle\dot{q_2}\rangle &= \frac{\langle p_2\rangle}{m_2},\\
\langle\dot{p_1}\rangle &= -m_1\omega_1^2\langle q_1\rangle + g_0\langle c^\dagger\rangle\langle c\rangle - g_c\langle q_2\rangle - \gamma_1\langle p_1\rangle,\\
\langle\dot{p_2}\rangle &= -m_2\omega_2^2\langle q_2\rangle - g_c\langle q_1\rangle - \gamma_2\langle p_2\rangle,\\
\langle\dot{c}\rangle &= -(\kappa + i\Delta_c)\langle c\rangle + i g_0\langle c\rangle\langle q_1\rangle - i g\langle a\rangle + E_l + \epsilon_p e^{-i\delta t},\\
\langle\dot{a}\rangle &= -(\gamma_a + i\Delta_a)\langle a\rangle - i g\langle c\rangle.
\end{aligned} \quad (4)$$

Here, Eq. (4) represents a set of nonlinear equations with mean values. The noise terms are vanished due to their zero mean values. To find out the steady-state values of the system, we define new operators with their steady states [79,80]. Therefore,

$$\langle o\rangle = o_s + o_+\epsilon_p e^{-i\delta t} + o_-\epsilon_p^\star e^{i\delta t}. \quad (5)$$

The first term in Eq. (5) on the right side represents the steady-state value, the second and third terms are treated as perturbations, respectively, with frequencies $\omega_l, \omega_p, 2\omega_l - \omega_p$. Substituting Eq. (5) into Eq. (4) using the steady-state condition $o = o_s + \delta o$ and $o_s \gg \delta o$. Keeping the first-order terms, the

steady-state mean values are described as

$$\begin{aligned} p_{1s} &= p_{2s} = 0, \\ q_{1s} &= \frac{g_0 \mid c_s \mid^2}{m_1\omega_1^2 - \frac{g_c^2}{m_2\omega_2^2}}, \\ q_{2s} &= \frac{-g_0 g_c \mid c_s \mid^2}{m_2\omega_2^2\left(m_1\omega_1^2 - \frac{g_c^2}{m_2\omega_2^2}\right)}, \\ c_s &= \frac{E_L}{\kappa + i\Delta + \frac{g^2}{\gamma_a + i\Delta_a}}, \\ \Delta &= \Delta_c - g_0 q_{1s}. \end{aligned} \tag{6}$$

Hence,

$$c_- = \epsilon_p[A - B + C - B^2(A' + B + C')^{-1}]^{-1}, \tag{7}$$

where

$$\begin{aligned} A &= \kappa + i(\Delta - \delta), \\ B &= \frac{G_s}{\alpha - \beta}, \\ \alpha &= m_1\left(\omega_1^2 - \delta^2 - i\delta\gamma_1\right), \\ \beta &= \frac{g_c^2}{m_2\left(\omega_2^2 - \delta^2 - i\delta\gamma_2\right)}, \\ G_s &= g_0^2 \mid c_s \mid^2, C = \frac{g_a^2}{\gamma_a + i(\Delta_a - \delta)}, \\ A' &= \kappa - i(\Delta + \delta), \\ C' &= \frac{g_a^2}{\gamma_a - i(\Delta_a + \delta)}. \end{aligned}$$

Here, c_- represents the analytic description of the optomechanical-induced transparency. It shows the nonlinearity behavior of the system. Moreover, we are dealing with the mean response of the system to the probe field at which $\Delta_c = \Delta_a$; in this case the atomic state remains in the excited state, which implies that the field frequency is in resonance with the atomic frequency, i.e., $\omega_c = \omega_a$. In addition, at detuning $\delta = \omega_{1,2}$ and $\Delta = \delta$, the coupling between the cavity field and MR_1 becomes stronger. For simplification, we consider that the system is in the resolved-sideband regime, i.e., $\omega_{1,2} \gg \kappa$ and $\delta \sim \omega_{1,2}$ [1]. We are interested in the outfield of the cavity, therefore we use the input and output relation of the cavity [81].

$$\begin{aligned} c_{\text{out}} &= \sqrt{2\kappa}c - c_{\text{in}}, \\ c_{\text{out}} &= \sqrt{2\kappa}\left(c_s - \frac{E_l}{\sqrt{2\kappa}}\right) + \sqrt{2\kappa}\left(c_- - \frac{\epsilon_p}{\sqrt{2\kappa}}\right)e^{-i\delta t} \\ &\quad + \sqrt{2\kappa}c_+ e^{i\delta t}. \end{aligned} \tag{8}$$

Equation (8) shows that the output field consists of three terms. The first term corresponds to the output field at driving field with amplitude E_l and frequency ω_l. The second term corresponds to the probe field with frequency ω_p and the last one corresponds to the output field with frequency $2\omega_l$-ω_p, which is related to the stoke field. Moreover, the second term represents the electromechanical-induced transparency, while the third term shows four-wave mixing of the system. In the four-wave mixing process the two photons of the driving field interact with a single photon of the probe field each with frequencies ω_l and ω_p born a new photon of frequency $2\omega_l$-ω_p. It shows the nonlinearity behavior of the system. We are interested in the outgoing field of the probe field. For this description, we write the rescaled output field corresponding to the probe field amplitude, i.e.,

$$E_{\text{out}} = \frac{\sqrt{2\kappa}c_-}{\epsilon_p}. \tag{9}$$

The output probe field accounts for in-phase and out-phase as part of real and imaginary parts corresponding to the quadratures $\text{Re}(E_{\text{out}}) = \frac{\kappa(c_- + c_-^*)}{\epsilon_p}$ and $\text{Im}(E_{\text{out}}) = \frac{\kappa(c_- - c_-^*)}{\epsilon_p}$, which describe the absorption and dispersion of the system with respect to the probe field. In general, modification of the probe field and induced transparency is produced by the atom-field coupling, and coupling of the mechanical resonator with the cavity [1,39]. Here, in the present case we discuss the electromagnetically induced transparency in detail in the presence of optomechanical coupling, atom coupling, and an electrostatic Coulomb coupling. Moreover, in the narrow regime of the optomechanical-transparency window the phase dispersion relation is $\phi_t(\omega_p) = \arg(E_{\text{out}})$ can cause the transmission group delay given by $\tau_g = \frac{d\phi_t(\omega_p)}{d(\omega_p)}$. The positive group delay $\tau_g > 0$ corresponds to fast light and the negative delay group $\tau_g < 0$ corresponds to slow light, respectively. The phase change can play a significant role in slow and fast light propagation, which is treated separately.

We select the parameter values used in this paper unless stated differently [1,27,41,82–84]. Here, $\omega_1 = \omega_2 = 2\pi \times 947$ KHz, $\kappa = 2\pi \times 215$ KHz, $Q = 6700$, $\gamma_{1,2} = \frac{\omega_{1,2}}{Q}$, $m_1 = m_2 = 145$ ng, $\delta = \omega_{1,2}$ typically $N_a = 10^6$ Rb^{87} atoms are coupled to the laser light inside a Fabery Perot cavity, with atomic decay rate $\gamma_a = 2\pi \times 10$ KHz. The wavelength of the driving field $\lambda_l = 1064$ nm, laser power $\wp_l = 2$ mW, length of the cavity $L = 25$ nm, $E_l = 2\pi \times 20 \times 10^5$ Hz. Moreover, atom-field coupling $g_{ac}\sqrt{N_a} = 2\pi \times 40$ KHz, the optomechanical coupling $g_0 = 2\pi \times 4$ KHz, and the Coulomb coupling $g_c = 2\pi \times 100$ KHz. The atomic detuning $\Delta_a = 2\pi \times 30$ KHz, and the field detuning $\Delta_c = 2\pi \times 100$ KHz.

IV. MULTIPLE-EMIT-WINDOWS PROFILE IN THE OUTPUT FIELD

In this section, we explain the multiple EMIT of the output probe field with frequency ω_p in the presence of atom-field interaction, mirror field interaction, and electrostatic Coulomb interaction. The output field of the probe field can be expressed as

$$E_{\text{out}} = \mu_p + i\nu_p, \tag{10}$$

where μ_p is the real part of the out field and ν_p is the imaginary part of the out field. We show real and imaginary profile of the output field in terms of the multiple-EMIT-windows profile. Likely, if both atom-field coupling and Coulomb coupling are switched, the single EMIT window profile is obtained [1,5]; if atom-field coupling or Coulomb coupling is switched, we get the double EMIT window profile [39,41]. Here, we describe EMIT in the presence of all three couplings.

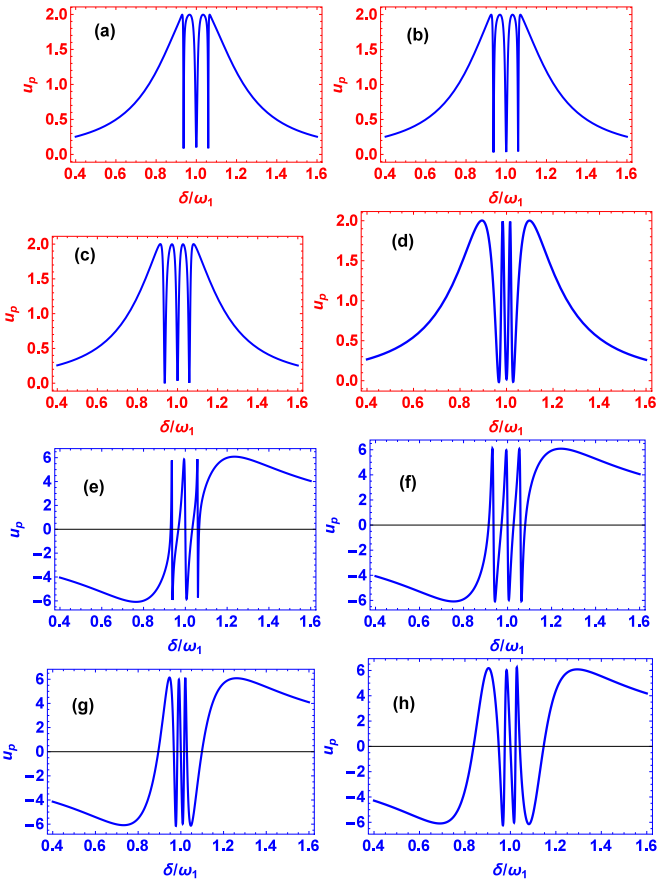

FIG. 2. We show the absorption Re[E_{out}] and dispersion Im[E_{out}] spectra of the output probe field as a function of normalized detuning $\frac{\delta}{\omega_1}$. (a) and (e) $g_0 = 2\pi \times 15$ KHz. (b) and (f) $g_0 = 2\pi \times 20$ KHz. (c) $g_0 = 2\pi \times 30$ KHz. Other parameters are $g_{ac} = 2\pi \times 40$ KHz, $g_c = 2\pi \times 100$ KHz, $\kappa = 2\pi \times 215$ KHz. (d), (g), and (h) g_0, g_{ac}, $g_c = 2\pi \times 50$ KHz, $2\pi \times 75$ KHz for comparable couplings.

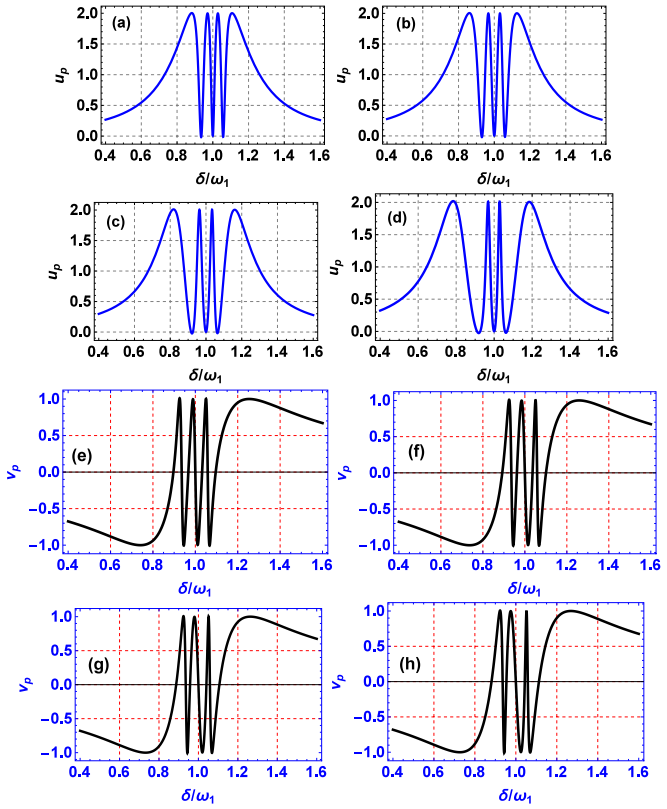

FIG. 3. We show the absorption Re[E_{out}] and dispersion Im[E_{out}] spectra of the output probe field as a function of normalized detuning $\frac{\delta}{\omega_1}$. (a) and (e) $g_{ac}\sqrt{N_a} = 2\pi \times 40$ KHz. (b) and (f) $g_{ac}\sqrt{N_a} = 2\pi \times 50$ KHz. (c) and (g) $g_{ac}\sqrt{N_a} = 2\pi \times 60$ KHz. (d) and (h) $g_{ac}\sqrt{N_a} = 2\pi \times 70$ KHz. The rest of the parameters are the same as those used in Fig. 2.

In Figs. 2(a)–2(h), we show the absorption Re[E_{out}] and dispersion Im[E_{out}] multiple EMIT profile of the out probe field as a function of normalized detuning δ/ω_1 for different values of optomechanical coupling. For simplification, we consider both mechanical resonators MR_1 and MR_2 to be identical. Later on, we will treat both MR_1 and MR_2 differently. The electromechanical-induced transparency is generated by the coupling between the MR_1 and optical field. The coupling between the MR_1 and optical field generates the radiation pressure force. This radiation force oscillating with frequency difference correspond to detuning, i.e., $\delta = \omega_p - \omega_l$. If this frequency approaches MR_1 resonance frequency ω_1, then the MR_1 mode starts to vibrate coherently. In this case the frequency of the probe field turns from Stoke frequency to anti-Stoke frequency $\omega_l + \omega_p$; it generates the light scattering inside the cavity of the strong driving field and produces destructive interference. In such a case the system is in the resolved side-banded regime at which $\omega_1 \gg \kappa$. Therefore, we consider the anti-Stoke field with frequency $\omega_l + \omega_p$ inside the cavity. It suppresses the intracavity probe field and as a result a narrow transparency window of the out field is produced. In short EMIT depends on both the constructive and destructive interferences. In Figs. 2(a)–2(c), we plot the absorption spectrum of the output field for weaker optomechanical coupling, i.e., $g_0 = 2\pi \times 10$ KHz, $2\pi \times 15$ KHz, $2\pi \times 20$ KHz. For these values the EMIT transparency windows are thinner at the sides while broader at the middle. By increasing the value of optomechanical coupling the EMIT multiple window become wider at the side and narrow at the middle. If we increase the value of optomechanical coupling g_0 to comparable values of g_{ac} and $g_c = 2\pi \times 50$ KHz. The EMIT windows become much wider at the side and much narrower at the middle as shown in Figs. 2(d)–2(g). In this case, we assume that there are the least number of atoms and low voltages across each mirror (weak charges). However, for higher comparable values of all three couplings for the high input field, a higher number of two-level atoms and maximum voltages (greater charges), i.e., g_0, g_{ac}, $g_c > 2\pi \times 50$ KHz. The EMIT dispersion window becomes broader and broader at the sides as well as at the middle as shown in Fig. 2(h). In Fig. 3, we show the absorption Re[E_{out}] and dispersion Im[E_{out}] multiple EMIT profile of the out probe field as a function of normalized detuning $\frac{\delta}{\omega_1}$ for different values of the atom field coupling. In Figs. 3(a) and 3(e), and 3(b) and 3(f) both the central and side windows are broader for the values $g_{ac}\sqrt{N_a} = 2\pi \times 40$ KHz and $g_{ac}\sqrt{N_a} = 2\pi \times 50$ KHz. But further the central windows become narrow and the side windows become wider in Figs. 3(c,g,d,h), for the values

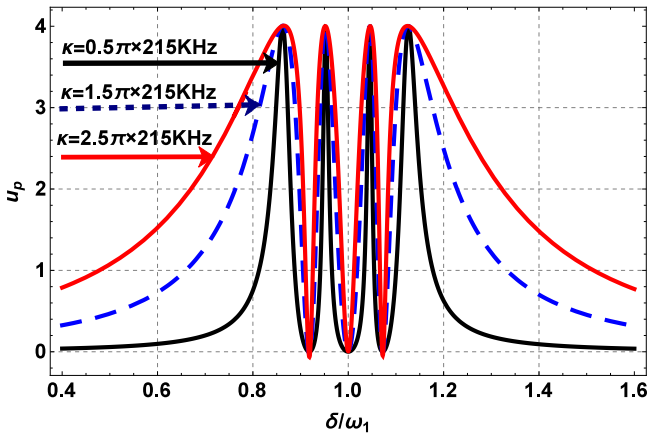

FIG. 4. The absorption Re$[E_{\text{out}}]$ as a function of normalized detuning $\frac{\delta}{\omega_1}$ corresponds to different values of cavity decay, $\kappa = 0.5\pi \times 215$ KHz (black solid line), $\kappa = 2.5\pi \times 215$ KHz (blue dotted line), $\kappa = 1.5\pi \times 215$ KHz (red solid line).

$g_{ac}\sqrt{N_a} = 2\pi \times 60$ KHz, $g_{ac}\sqrt{N_a} = 2\pi \times 70$ KHz. In short both the EMIT absorption and dispersion window profiles are wider at the center and narrow on the side for minimum values of the coupling constant and vice versa. In Fig. 4, the absorption Re$[E_{\text{out}}]$ is shown for different values of κ. The absorption spectrum has three maxima and two minima. The maxima and minima of the window remains unchanged for different values of κ. The minima of the EMIT window profile of the transparency become narrow and sharper for higher values of κ but the maxima of the window become wider and broaden for higher values of the cavity decay. Moreover, for a fixed laser driving field, where the κ value is higher the spectrum becomes wider and wider at either side. But, in contrast, the central spectrum becomes narrower and narrower for higher values of κ. The central line of the absorption spectra of Re$[E_{\text{out}}]$ is helpful in detecting the electrostatic interaction between the MR_s. In Fig. 5, we show the absorption Re$[E_{\text{out}}]$ spectrum as a function of normalized $\frac{\delta}{\omega_1}$ for different values of Coulomb coupling g_c. In the absence of atom field coupling the EMIT window profile splits into two windows [40,41]. Once the atom field coupling is present the EMIT window profile splits into the three-window profile. We see from Figs. 5(a)–5(c) plotted for minimum values of Coulomb coupling the EMIT window profile is in closer form. But the EMIT window profile in Figs. 5(d)–5(g) become wider and wider once we increase the values of the Coulomb coupling. Our system is more effective as discussed in previous work [41,85,86]. In our proposed system, the most sensitive terms are the atom field coupling g_{ac}, cavity decay κ, and Coulomb coupling g_c. The result of Re$[E_{\text{out}}]$ against robustness κ and the narrow profile of the out probe field. In such a situation, we can measure the coupling strength with more precision between the MR_s. Our robustness system consists of the fixed value of the Coulomb coupling, atom field coupling, and the input driving field by which the equilibrium position of the mechanical resonator may decide. Increasing the value of κ causes the radiation pressure to decrease. But, when the MR is at large displacement large strain is needed to reduce the radiation pressure and vice versa. Moreover, the Coulomb coupling can break the symmetry of

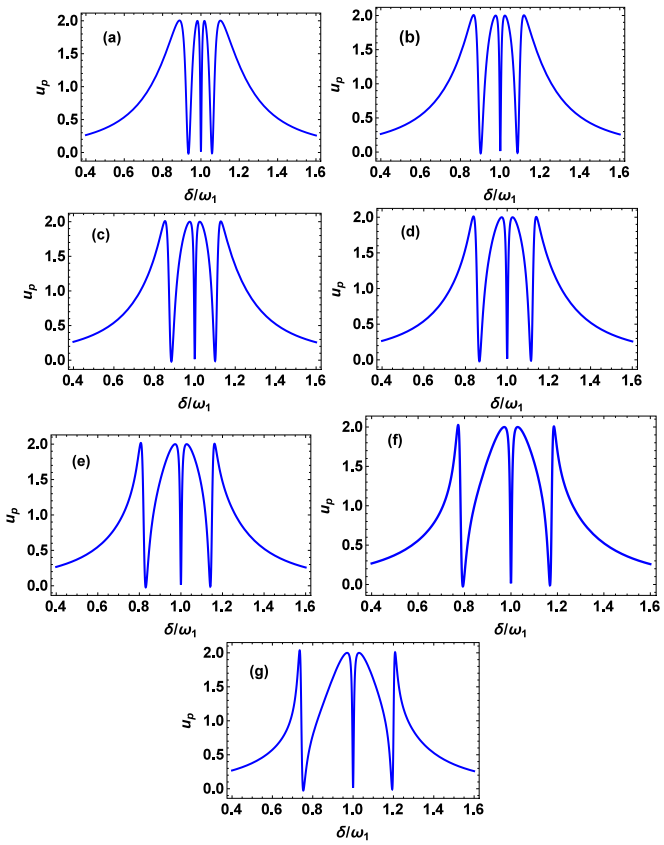

FIG. 5. We show the absorption Re$[E_{\text{out}}]$ spectrum as a function of normalized detuning $\frac{\delta}{\omega_1}$ for different values of Coulomb coupling. (a) $g_c = 2\pi \times 100$ KHz, (b) $g_c = 3\pi \times 100$ KHz, (c) $g_c = 4\pi \times 100$ KHz, (d) $g_c = 5\pi \times 100$ KHz, (e) $g_c = 6\pi \times 100$ KHz, (f) $g_c = 7\pi \times 100$ KHz, (g) $g_c = 8\pi \times 100$ KHz. Other parameters are $g_{ac}\sqrt{N_a} = 2\pi \times 40$ KHz, $g_0 = 2\pi \times 4$ KHz, $\kappa = 2\pi \times 215$ KHz.

the EMIT interference, produce a bright shape within the EMIT line, and generate double and triple EMIT windows of the out field. Further, the absorption and dispersion spectrum becomes narrow for large displacement. Therefore, the system needs to be robust against cavity decay κ.

V. DIFFERENT MECHANICAL RESONATORS

A. When frequencies of MR_1 and MR_2 $\omega_1 \neq \omega_2$

Now, we treated the MR_1 and MR_2 as different oscillators having different frequencies $\omega_1 \neq \omega_2$. In this case the result is a little different from identical MR_1 and MR_2. In Fig. 6 the absorption spectrum Re$[E_{\text{out}}]$ of triple EMIT shows against the normalized detuning $\frac{\delta}{\omega_1}$ identical MR_s. It shows the comparison of two different MR_s to two identical MR_s. In the case of identical MR_s the coupling constant is less sensitive as compared to different MR_s. For different oscillators $\omega_1 \neq \omega_2$ the spectrum lines shift towards right while in the case of same resonators $\omega_1 = \omega_2$ the spectrum lines move towards left. We take the robustness of our system in the resolved-sideband regime in which $\omega_1 \gg \kappa$. Moreover, the multiple EMIT windows work in the resolved-sideband regime in which the bright lines appeared. In the unresolved-sideband regime

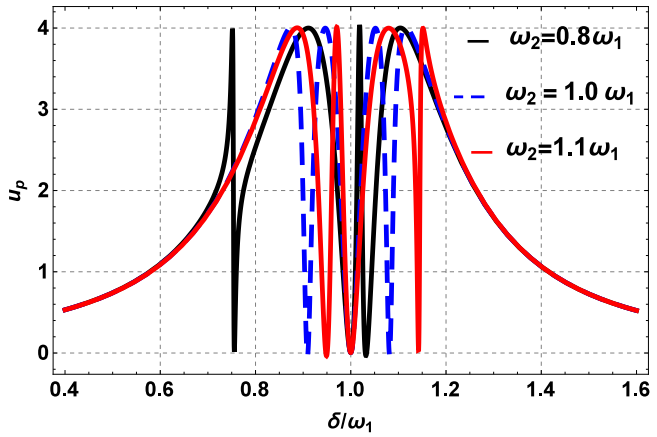

FIG. 6. The absorption spectrum Re$[E_{\text{out}}]$ as a function of normalized detuning $\frac{\delta}{\omega_1}$ identical resonators correspond to different frequencies of MR_s.

$\omega_1 \ll \kappa$ the system is not robust and the absorption spectrum of EMIT does not work and the sideband transition looks blurred.

B. When the masses of MR_1 and MR_2 $m_1 \neq m_2$

In Fig. 7, we show the normalized absorption Re$[E_{\text{out}}]$ spectrum of the triple EMIT window profile versus normalized detuning $\frac{\delta}{\omega_1}$ identical resonators corresponding to different masses. In this case, if the masses of the mechanical resonators are smaller the multiple-EMIT-windows profile is wider on both the left and right sides. By increasing the mass of one resonator corresponding to the other resonator the multiple-EMIT-windows profile moves from both sides towards the center and comes closer to each other. Both maxima and minima peak heights remain unchanged. The sharpness of the peaks of both maxima and minima remains the same on both sides. But the central peaks of both maxima and minima become sharper (red one) with increasing the mass of a resonator. The absorption power increases by increasing the masses of the resonators. In this case the radiation pressure does not increase inside the cavity. In this way, we can

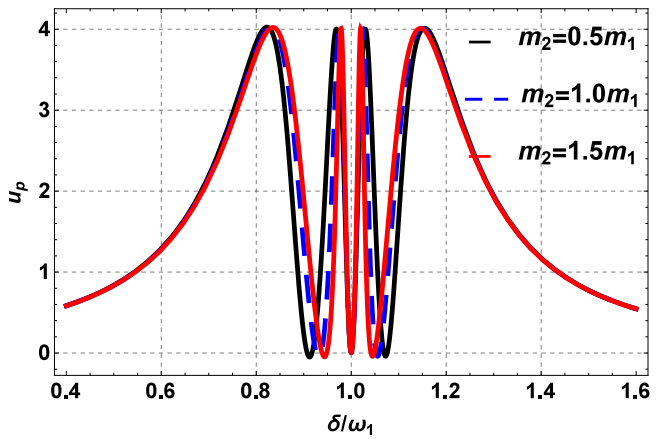

FIG. 7. The absorption spectrum Re$[E_{\text{out}}]$ as a function of normalized detuning $\frac{\delta}{\omega_1}$ identical resonators correspond to different masses of MR_1 and MR_2.

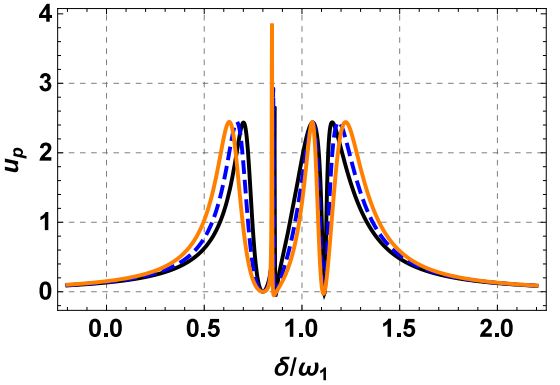

FIG. 8. The absorption of the output field as a function of normalized detuning $\frac{\delta}{\omega_1}$ shows the multiple Fano resonances correspond to different values of atom field coupling, $g_{ac}\sqrt{N_a} = 2\pi \times$ 10 KHz (black solid line), $g_{ac}\sqrt{N_a} = 2\pi \times 20$ KHz (blue dashed line), $g_{ac}\sqrt{N_a} = 2\pi \times 30$ KHz (orange solid line). The other parameters are $\kappa = 2\pi \times 215$ KHz, $\Delta_a = 2\pi \times 100$ KHz, and $g_0 = 2\pi \times 8$ KHz.

handle the optomechanical coupling strength by reducing the radiation pressure inside the cavity with changing the mass of one resonator to the other resonator. On the other hand the symmetry of the system also remains unchanged by handling the nano-electro-optomechanical coupling.

VI. MULTIPLE FANO RESONANCES IN THE OUTPUT FIELD

In this section, we demonstrate the Fano line shapes by using certain conditions of [52] in multiple electrical-induced-transparency results of the output field. Since Fano resonances are produced by the constructive and destructive interferences between the probe field and driving field amplitudes. By switching off both the Coulomb coupling and atom field coupling a single Fano resonance (SFR) appeared while switching off one of the couplings of NEOMS there is a double Fano resonance (DFR) which is discussed in detail [39,52]. Here, we discuss the multiple Fano resonances (MFR) in hybrid nano-electro-optomechanics system (NEOMS) in the presence of all the couplings. In Figs. 8 and 9, we show narrow Fano resonance profiles of the output field in their absorption and dispersion forms. It can be observed to broaden at detuning $\Delta_a \sim \omega_{1,2}$. In Fig. 7, we take the values of $\Delta_a = 2\pi \times$ 100 KHz, $\delta = 2\pi \times 947$ KHz, $\Delta = \omega_{1,2}$, $g_c = 2\pi \times 100$ KHz, $g_0 = 2\pi \times 8$ KHz. The Fano resonance moves away from the cavity resonance and for higher values at off resonance it acquires an asymmetric line shapes. The peaks and depth of lines become steeper and broaden shape for different values of the atom field coupling via keeping the Coulomb coupling fixed. The Fano line shape occurs when the system is in complete resonance. The existence of two-level atoms leads to nonresonant interaction; as a result the Fano line shapes transfer from symmetric to antiasymmetric shapes. Moreover, when the atoms are in resonant with the stokes sideband the absorption peaks of the EMIT can split due to the vacuum Rabi frequency $g_{ac}\sqrt{N_a}$ as shown in Fig. 8. In short, from Figs. 8 and 9, it is clear that in the presence of all three couplings of

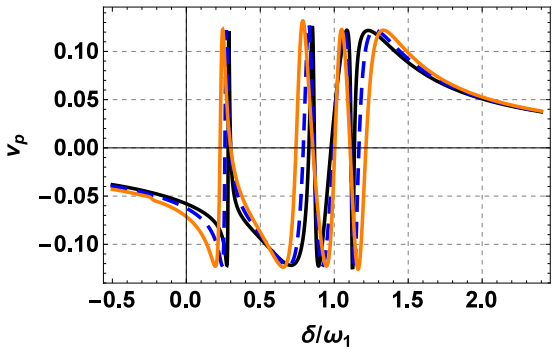

FIG. 9. Multiple Fano resonance profiles of the output field as a function of normalized detuning $\frac{\delta}{\omega_1}$ show the multiple Fano resonances corresponding to different values of atom field coupling, $g_{ac}\sqrt{N_a} = 2\pi \times 10$ KHz (black solid line), $g_{ac}\sqrt{N_a} = 2\pi \times 20$ KHz (blue dashed line), $g_{ac}\sqrt{N_a} = 2\pi \times 30$ KHz (orange solid line).

the NEOMS, we observed the sharp and broadened multiple Fano resonances (MFR) in the system.

VII. CONCLUSION

In conclusion, we demonstrated the multiple-EMIT-windows profile under the Coulomb coupling between the charged mechanical resonators in the presence of a medium consisting of two-level atoms. The atom-atom interaction is low so that we have each atom acting individually. This is our first proposed model for multiple EMIT under the Coulomb interaction and the two-level atoms with the Jaynen's Cumming model. This work can be extended into other multiple interactions such as dipole-dipole interaction between the charged resonators, long-range interaction, ion-ion Coulomb interaction and van der Waals interaction. We discuss the robustness of our system and provide the suggestion for the detection of Coulomb coupling in the multiple-EMIT-windows profile. We provide an analytical approach for the multiple-EMIT-windows profile. We discuss in detail the results for the same resonators and for different resonators. We show the behavior of the system under different masses of resonators. We studied Coulomb coupling and atom field interaction separately and discuss the effects of each individually. We report the multiple Fano resonances in hybrid NEOMS by adjusting all the coupling with one another. We report that, when the atoms are resonant with the anti-Stokes sideband of the peaks of the multiple-EMIT-windows profile transfer from symmetric shapes to antisymmetric Fano resonances.

ACKNOWLEDGMENTS

The authors thank RIKEN and UEC, Tokyo, Japan for a conducive support to complete the manuscript.

[1] G. S. Agarwal and S. Huang, Phys. Rev. A **81**, 041803 (2010).
[2] S. E. Harris, J. E. Field, and A. Imamoğlu, Phys. Rev. Lett. **64**, 1107 (1990).
[3] K.-J. Boller, A. Imamoğlu, and S. E. Harris, Phys. Rev. Lett. **66**, 2593 (1991).
[4] J. E. Field, K. H. Hahn, and S. E. Harris, Phys. Rev. Lett. **67**, 3062 (1991).
[5] S. Weis, R. Riviere, S. Deleglise, E. Gavartin, O. Arcizet, A. Schliesser, and T. J. Kippenberg, Science **330**, 1520 (2010).
[6] B. Chen, C. Jiang, and K.-D. Zhu, Phys. Rev. A **83**, 055803 (2011).
[7] M. C. Phillips, H. Wang, I. Rumyantsev, N. H. Kwong, R. Takayama, and R. Binder, Phys. Rev. Lett. **91**, 183602 (2003).
[8] X. Xu *et al.*, Nat. Phys. **4**, 692 (2008).
[9] N. Liu *et al.*, Nat. Mater. **8**, 758 (2009).
[10] C. Santori, P. Tamarat, P. Neumann, J. Wrachtrup, D. Fattal, R. G. Beausoleil, J. Rabeau, P. Olivero, A. D. Greentree, S. Prawer, F. Jelezko, and P. Hemmer, Phys. Rev. Lett. **97**, 247401 (2006).
[11] E. Cabelly, C. L. Garrido Alzar *et al.*, Am. J. Phys. **70**, 37 (2002).
[12] P. Tassin, Lei Zhang, Th. Koschny, E. N. Economou, and C. M. Soukoulis, Phys. Rev. Lett. **102**, 053901 (2009).
[13] L. He, Y. X. Liu, S. Yi, C. P. Sun, and F. Nori, Phys. Rev. A **75**, 063818 (2007).
[14] F. Bariani, S. Singh, L. F. Buchmann, M. Vengalattore, and P. Meystre, Phys. Rev. A **90**, 033838 (2014); F. Bariani, H. Seok, S. Singh, M. Vengalattore, and P. Meystre, *ibid.* **92**, 043817 (2015).
[15] S. Huang and M. Tsang, arXiv:1403.1340.
[16] Z. L. Xiang, S. Ashhab, J. Q. You, and F. Nori, Rev. Mod. Phys. **85**, 623 (2013).
[17] D. Rugar, R. Budakian, H. J. Mamin, and B. W. Chui, Nature (London) **430**, 329 (2004).
[18] Y. X. Liu, A. Miranowicz, Y. B. Gao, J. Bajer, C. P. Sun, and F. Nori, Phys. Rev. A **82**, 032101 (2010).
[19] H. Xiong, L. G. Si, X. Y. Lu, X. X. Yang, and Y. Wu, Opt. Lett. **38**, 353 (2013).
[20] T. J. Kippenberg and K. J. Vahala, Opt. Express **15**, 17172 (2007).
[21] F. Marquardt and S. M. Girvin, Physics **2**, 40 (2009).
[22] M. Aspelmeyer, P. Meystre, and K. Schwab, Phys. Today **65**, 29 (2012).
[23] M. J. Akram, M. M. Khan, and F. Saif, Phys. Rev. A. **92**, 023846 (2015).
[24] S. Huang and G. S. Agarwal, Phys. Rev. A. **80**, 033807 (2009).
[25] S. Shahidani, M. H. Naderi, and M. Soltanolkotabi, J. Mod. Opt. **62**, 114 (2015).
[26] J. M. Dobrindt, I. Wilson-Rae, and T. J. Kippenberg, Phys. Rev. Lett. **101**, 263602 (2008).
[27] M. S. Groblacher, K. Hammerer, and M. R. Aspelmeyer, Nature (London) **460**, 724 (2009).
[28] T. J. Kippenberg, H. Rokhsari, T. Carmon, A. Scherer, and K. J. Vahala, Phys. Rev. Lett. **95**, 033901 (2005).
[29] T. Carmon, H. Rokhsari, L. Yang, T. J. Kippenberg, and K. J. Vahala, Phys. Rev. Lett. **94**, 223902 (2005).
[30] F. Saif and M. Asjad, Optik: International Journal of Light and Electron Optics **125**, 5455 (2014).
[31] C. H. Dong, V. Fiore, M. C. Kuzyk, and H. L. Wang, Science **338**, 1609 (2012).
[32] M. Asjad and F. Saif, Phys. Rev. A **84**, 033606 (2011); Phys. Lett. A **376**, 2608 (2012).

[33] M. Asjad, M. A. Shahzad, and F. Saif, Eur. Phys. J. D **67**, 198 (2013).

[34] M. J. Akram and F. Saif, Nonlinear Dynamics **83**, 963 (2016).

[35] M. Ayub, K. Ammar, and F. Saif, Int. J. Laser Phys. **24**, 115503 (2014).

[36] K. A. Yasir, M. Ayub, and F. Saif, J. Mod. Opt. **61**, 1318 (2014).

[37] H. Jing, Ş. K. Özdemir, Z. Geng, J. Zhang, X.-Y. Lü, B. Peng, L. Yang, and F. Nori, Sci. Rep. **5**, 9663 (2015); Q. Wu, J.-Q. Zhang, J.-H. Wu, M. Feng, and Z.-M. Zhang, Opt. Express **23**(14), 18534 (2015).

[38] S. Haroche and J. M. Raimond, *Exploring the Quantum: Atoms, Cavities and Photons* (Oxford University Press, New York, 2006).

[39] M. J. Akram, F. Ghafoor, and F. Saif, J. Phys. B: At. Mol. Opt. Phys. **48**, 065502 (2015).

[40] P. C. Ma, L. L. Yan, G. B. Chen, X. W. Li, and Y. B. Zhan, Laser Phys. Lett. **13**, 125301 (2016).

[41] P. C. Ma, J. Q. Zhang, Y. Xiao, M. Feng, and Z.-M. Zhang, Phys. Rev. A **90**, 043825 (2014).

[42] R. X. Chen, L. T. Shen, and S. B. Zheng, Phys. Rev. A **91**, 022326 (2015).

[43] A. Nunnenkamp, K. Borkje, and S. M. Girvin, Phys. Rev. Lett. **107**, 063602 (2011).

[44] J. Q. Liao, H. K. Cheung, and C. K. Law, Phys. Rev. A **85**, 025803 (2012).

[45] J. Q. Liao and F. Nori, Phys. Rev. A **88**, 023853 (2013).

[46] A. Kronwald, M. Ludwig, and F. Marquardt, Phys. Rev. A **87**, 013847 (2013).

[47] S. Gupta, K. L. Moore, K. W. Murch, and D. M. Stamper-Kurn, Phys. Rev. Lett. **99**, 213601 (2007).

[48] M. Eichenfield, J. Chan, R. M. Camacho, K. J. Vahala, and O. Painter, Nature (London) **462**, 78 (2009).

[49] J. D. Teufel, D. Li, M. S. Allman, K. Cicak, A. J. Sirois, J. D. Whittaker, and R. W. Simmonds, Nature (London) **471**, 204 (2011).

[50] U. Fano, Nuovo Cim **12**, 154 (1935); Phys. Rev. **50**, 573 (1936); **51**, 288 (1937); Ann. Phys. **424**, 393 (1938); J. Opt. Soc. Am. **31**, 213 (1941).

[51] U. Fano, Phys. Rev. **124**, 1866 (1961).

[52] K. Qu and G. S. Agarwal, Phys. Rev. A **87**, 063813 (2013).

[53] B. Gallinet and O. J. F. Martin, ACS Nano **5**, 8999 (2011); Phys. Rev. B **83**, 235427 (2011).

[54] Y. Francescato, V. Giannini, and S. A. Maier, ACS Nano **6**, 1830 (2012); A. Artar, Y. Ahmet Ali, and H. Altug, Nano Lett. **11**, 3694 (2011).

[55] M. V. Rybin, A. B. Khanikaev, M. Inoue, K. B. Samusev, M. J. Steel, G. Yushin, and M. F. Limonov, Phys. Rev. Lett. **103**, 023901 (2009).

[56] S. Nojima, M. Usuki, M. Yawata, and M. Nakahata, Phys. Rev. A **85**, 063818 (2012).

[57] G. L. Shang *et al.*, Sci. Rep. **4**, 3601 (2014).

[58] S. Sasaki, H. Tamura, T. Akazaki, and T. Fujisawa, Phys. Rev. Lett. **103**, 266806 (2009).

[59] I. V. Iorsh, I. V. Shadrivov, P. A. Belov, and Yuri S. Kivshar, Phys. Rev. B **88**, 195422 (2013).

[60] J. Guo, L. Jiang, Y. Jia, X. Dai, Y. Xiang, and D. Fan, Opt. Express **25**, 5972 (2017).

[61] M. O. Scully, K. R. Chapin, K. E. Dorfman, M. B. Kim, and A. A. Svidzinsky, Proc. Natl. Acad. Sci. USA **108**, 15097 (2011).

[62] A. E. Miroshnichenko, S. Flach, and Y. S. Kivshar, Rev. Mod. Phys. **82**, 2257 (2010).

[63] F. Hocke, X. Zhou, A. Schliesser, T. J. Kippenberg, H. Huebl, and R. Gross, New J. Phys. **14**, 123037 (2012).

[64] H. Ritsch, P. Domokos, F. Brennecke, and T. Esslinger, Rev. Mod. Phys. **85**, 553 (2013).

[65] A. H. Safavi-Naeini, T. P. M. Alegre, J. Chan, M. Eichenfield, M. Winger, Q. Lin, J. T. Hill, D. Chang, and O. Painter, Nature (London) **472**, 69 (2011).

[66] M. Karuza, C. Biancofiore, M. Bawaj, C. Molinelli, M. Galassi, R. Natali, P. Tombesi, G. Di Giuseppe, and D. Vitali, Phys. Rev. A **88**, 013804 (2013).

[67] H. Xiong, L. G. Si, A. S. Zheng, X. Yang, and Y. Wu, Phys. Rev. A **86**, 013815 (2012).

[68] Q. Wang, L. Yan, P. C. Ma, Z. He, and C. M. Yao, Eur. Phys. J. D **69**, 213 (2015).

[69] C. Jiang, H. Liu, Y. Cui, X. Li, G. Chen, and B. Chen, Opt. Express **21**(10), 12165 (2013).

[70] L. Giner, L. Veissier, B. Sparkes, A. S. Sheremet, A. Nicolas, O. S. Mishina, M. Scherman, S. Burks, I. Shomroni, D. V. Kupriyanov, P. K. Lam, E. Giacobino, and J. Laurat, Phys. Rev. A **87**, 013823 (2013).

[71] Y. Xiao, Y.-F. Yu, and Z.-M. Zhang, Opt. Express **22**, 17979 (2014).

[72] M. Tavis and F. W. Cummings, Phys. Rev. **170**, 379 (1968).

[73] T. Holstein and H. Primakoff, Phys. Rev. **58**, 1098 (1940).

[74] L. Tian and P. Zoller, Phys. Rev. Lett. **93**, 266403 (2004).

[75] W. K. Hensinger, D. W. Utami, H. S. Goan, K. Schwab, C. Monroe, and G. J. Milburn, Phys. Rev. A **72**, 041405(R) (2005).

[76] C. N. Ren, J. Q. Zhang, L. B. Chen, and Y. J. Gu, Opt. Express **23**, 18545 (2016).

[77] C. Genes, D. Vitali, P. Tombesi, S. Gigan, and M. Aspelmeyer, Phys. Rev. A **77**, 033804 (2008).

[78] C. W. Gardiner and P. Zoller, *Quantum Noise* (Springer-Verlag, Berlin, 1991).

[79] R. W. Boyd, *Nonlinear Optics* (Academic Press, New York, 2010).

[80] J. Q. Zhang, Y. Li, M. Feng, and Y. Xu, Phys. Rev. A **86**, 053806 (2012).

[81] D. F. Walls and G. J. Milburn, *Quantum Optics* (Springer-Verlag, Berlin, 1994).

[82] H. Wang, Z. Wang, J. Zhang, Ş. K. Özdemir, L. Yang, and Y.-x. Liu, Phys. Rev. A **90**, 053814 (2014).

[83] C. Genes, D. Vitali, and P. Tombesi, Phys. Rev. A. **77**, 050307 (2008).

[84] L. Li, W. Nie, and A. Chen, Nature Scientific Report. **6**, 35090 (2016).

[85] J. J. Li and K. D. Zhu, Appl. Phys. Lett. **94**, 063116 (2009).

[86] W. He, J. J. Li, and K. D. Zhu, Opt. Lett. **35**, 339 (2010).